Stability Boundary for Haptic Rendering: Influence of Physical Damping

Thomas Hulin, Carsten Preusche and Gerd Hirzinger
German Aerospace Center (DLR)
Institute of Robotics and Mechatronics
D-82234 Wessling, Germany
Email: Thomas.Hulin@dlr.de

***Abstract*— Physical damping is increasing the z-width of haptic simulations. This paper derives the normalized stability boundaries for physically damped one degree of freedom haptic devices colliding with a virtual wall represented as spring-damper system. These boundaries are independent of the haptic device's mass and the sampling time. Furthermore, the dependency of the maximum stable virtual stiffness is discussed. Moreover, this paper illustrates that the passive region which is defined by Colgate's passivity condition is a subset inside the stable region for undelayed systems, but not for delayed systems.**

***Index Terms*— Haptic Rendering, Physical Damping, Stability Boundary, Normalized Haptic Parameters, Impedance Control**

I. Introduction

An elementary prerequisite for haptic applications is to preserve stability. Numerous theoretical and experimental approaches have been presented in the past that have dealt with ensuring stability for haptic interfaces. The passivity condition of Colgate, et al. in [1] and [2] represents one of the most cited theoretical studies towards a common stability condition. Although ensuring passivity of haptic devices is a general approach, it has the disadvantages of being conservative in terms of stability and requiring the presence of a mechanical damping.

A more accurate approach was introduced by Hannaford, et al. [3], [4], [5] with their time-domain passivity controller. They introduced a variable damper which eliminates the energy after it was generated by the haptic device.

The exact stability region for haptic walls represented by a virtual spring-damper system was first determined by Salcudean and Vlaar [6]. They considered their haptic device as a simple mass which is actuated by an one sample-step delayed force. Hence, it is controlled according to impedance causality. For this simplified control loop, they found the stability boundary inside a normalized parameter plane. The human operator was ignored for the stability analysis, as he tends to stabilize the system [7], [8]. In [9] this approach is enhanced by specifying the time delay as parameter. Furthermore, different control rules are compared inside the stable regions for undelayed and one sample step delayed force.

As discovered experimentally, the stable region can be increased if the haptic device is physically damped [2], [10]. Yet, theoretical investigations for the stability of physically damped haptic devices are rare and exist mainly for specific devices, e.g. [8].

This work was partly supported by the VRLab of the Volkswagen AG.

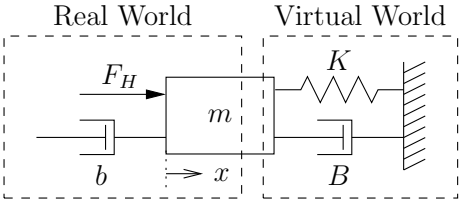

Fig. 1. The haptic device modeled as a damped mass m combined with a virtual spring and damper.

The present publication presents the normalized stability boundaries for haptic devices which are considered as a physically damped mass that is colliding with a virtual wall represented by a spring-damper system. First, a normalized characteristic equation of the system is derived that is independent of the haptic device's mass and the sampling time. It is used for determining the stability boundaries for several values of the physical damping. These results are compared to the passivity condition of Colgate, et al. [1], [2]. Finally, the dependency of the maximum stable virtual stiffness on the physical parameters of the haptic interface is discussed.

II. Problem Description

The typical implementation of a virtual wall in haptic simulations consists of a virtual spring and damper. The problem that occurs when using this representation is that virtual springs and dampers can be active in contrast to their real counterparts.

The active behavior has its origin mainly in the finite sampling rate and possible time delays, which occur particularly in teleoperation tasks. In haptic virtual reality simulations time delays may be caused e.g. by the force computation in the virtual world or by communication delays between the computer and the haptic device. Other sources for the active behavior can be a limited resolution of the haptic device's sensors and actuators, a compliance of the haptic display or noisy signals. Yet, this publication considers only the effects caused by the finite sampling rate and the time delays.

As it is shown in Fig. 1, the haptic device is represented by a damped mass. The dynamics of the actuators of the haptic

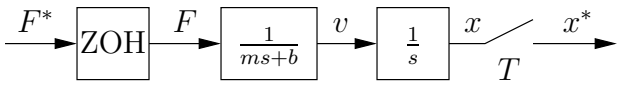

Fig. 2. Transfer function of physically damped mass m.

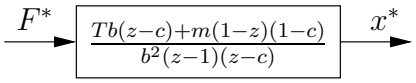

Fig. 3. Discrete-time transfer function which is equivalent to the system shown in Fig. 2.

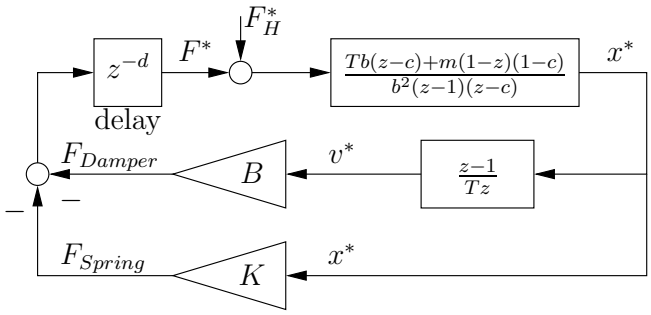

Fig. 4. Discrete-time control loop.

display are neglected, such that the force F of the virtual world can be assumed to be constant over one sampling period T.

For impedance control the worst-case scenario for stability is the situation when the operator is not grabbing the haptic device [7], [8]. Thus, the human operator is not taken into account in the following ($F_H = 0$). A system which is then found to be stable will be also stable if the operator is interacting with the device.

III. Discrete-Time Equivalent of the Damped Mass Transfer Function

The exact computation of the stability boundary for the system described in the previous section is non-trivial, as the system consists of both, continuous-time and discrete-time elements.

Recently, in [9], this problem was solved for physically undamped systems, where $b = 0$. To compute the stability boundary, a discrete-time equivalent of the mass transfer function was determined first. With it, the characteristic polynomial of the resulting discrete-time control loop could be easily calculated. Finally, the stability boundaries were determined iteratively using the characteristic polynomial.

The same approach is applicable for the damped mass system of Fig. 1. In the following, the discrete-time transfer function equivalent of the damped mass m shown in Fig. 2 will be calculated first, to determine the closed-loop characteristic polynomial subsequently.

A. Velocity

The discrete transfer function from the force F to the velocity $v = \dot{x}$ can be calculated by considering the differential equation of the damped mass m,

$$F = b\dot{x} + m\ddot{x} \tag{1}$$

where b is the physical (continuous-time) damping of the mass. For a constant force $F = const.$ the differential equation can be easily solved,

$$v(t) = v_\infty - (v_\infty - v_0)e^{-tb/m} \tag{2}$$

with $v_\infty = F/b$. For discrete-time systems the velocity at $t = k \cdot T$, with $k = 0, 1, 2, ...$ has to be computed. By assuming that the force is not changing during one sampling period T yields

$$v_{k+1} = cv_k + (1 - c)\frac{F_k}{b} \tag{3}$$

with

$$c = e^{-Tb/m}. \tag{4}$$

Thus, the exact transfer function from the force to the velocity is

$$H_v(z) = \frac{v}{F} = \frac{1 - c}{b(z - c)}. \tag{5}$$

B. Position

Out of the velocity v the position x results as integral

$$x(t) = \int_0^t v(\tau)d\tau. \tag{6}$$

For $0 \leq t < T$ the force F is constant. Thus, with equation (2) the integration of one sampling step yields

$$x(T) = \frac{F}{b}T + \frac{m}{b}(v_0 - \frac{F}{b})(1 - c). \tag{7}$$

Transferring this result into the discrete-time yields

$$x_{k+1} = x_k + \frac{F_k}{b}T + \frac{m}{b}(v_k - \frac{F_k}{b})(1 - c). \tag{8}$$

Hence, the exact transfer function from the force to the position (see Fig. 3) is

$$\begin{aligned} H_x(z) = \frac{x}{F} &= \frac{Tb(z - c) + m(1 - z)(1 - c)}{b^2(z - 1)(z - c)} \\ &= \frac{T}{b(z - 1)} - \frac{m(1 - c)}{b^2(z - c)}. \end{aligned} \tag{9}$$

With this discrete function, the closed loop behavior of the damped mass interacting with the virtual world can be investigated in the z-plane. The virtual world is simulated as spring-damper system (Fig. 1) which is equivalent to a discrete PD-controller.

C. Closed-loop transfer function

The resulting discrete-time control loop of the damped mass and the virtual world is shown in Fig. 4. With it, the transfer function $G(z)$ from force F_H^* to position x^* can be easily determined to be

$$G_x(z) = \Big(\big(-Tb+m(1-c)\big)z+\big(Tbc-m(1-c)\big)\Big)Tz^{1+d}\,/p(z) \tag{10}$$

with the characteristic polynomial

$$\begin{aligned} p(z) &= \Big(\big(m(1-c)-Tb\big)(KT+B)\Big)z^2 \\ &+\Big(\big(Tbc-m(1-c)\big)KT+\big(Tb+Tbc-2m(1-c)\big)B\Big)z \\ &-Tb^2(z-c)(z-1)z^{1+d}+\big(-Tbc+m(1-c)\big)B \end{aligned} \tag{11}$$

where K is the virtual stiffness, B the virtual damping and d the delay factor.

Remark 1: This equation corresponds to the one found by Gil et al. [8] for undelayed systems $d = 0$.

Remark 2: For physically undamped systems $b = 0$ yields for the discrete-time transfer functions (5) and (9)

$$\lim_{b\to 0} H_v(z) = \frac{T}{m(z-1)} \tag{12}$$

$$\lim_{b\to 0} H_x(z) = \frac{T^2(1+z)}{2m(z-1)^2} \tag{13}$$

This corresponds to the results determined in [9].

IV. Normalized Variables

In [6] and [9] normalized variables for the virtual stiffness and damping were introduced to simplify the characteristic polynomial of mechanically undamped haptic devices, such that the sampling time T and the mass m dropped out. In [9] the normalized variables were defined as

$$\begin{aligned} \alpha &= K\cdot T^2/m \quad &&\text{: normalized (virtual) stiffness} \\ \beta &= B\cdot T/m \quad &&\text{: normalized (virtual) damping} \end{aligned} \tag{14}$$

Applying these normalization rules to the characteristic polynomial (11) yields

$$\begin{aligned} p(z) &= \Big((1-c-Tb/m)(\alpha+\beta)\Big)z^2 \\ &+\Big((Tbc/m-1+c)\alpha+((1+c)Tb/m-2(1-c))\beta\Big)z \\ &-T^2b^2/m^2(z-c)(z-1)z^{1+d}+(-Tbc/m+(1-c))\beta. \end{aligned} \tag{15}$$

Obviously, the physical damping b depends linearly on m/T. Thus, introducing a new normalized parameter, namely the normalized physical damping

$$\delta \;=\; b\cdot T/m \tag{16}$$

simplifies the characteristic polynomial to

$$\begin{aligned} p(z) &= (1-c-\delta)(\alpha+\beta)\,z^2 \\ &+ \big((c\delta-1+c)\alpha+((1+c)\delta-2(1-c))\beta\big)z \\ &- \delta^2(z-c)(z-1)z^{1+d}+(1-c-c\delta)\beta \end{aligned} \tag{17}$$

with

$$c = e^{-\delta}. \tag{18}$$

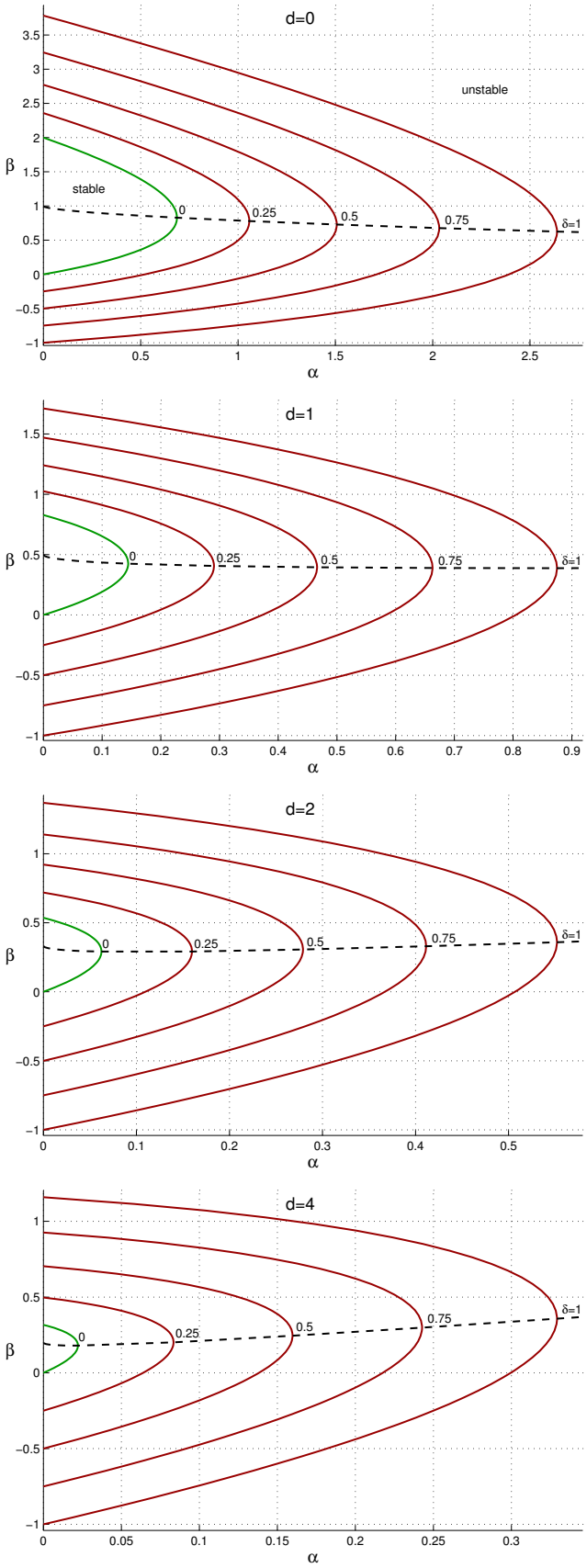

Fig. 5. The stability boundaries in the (α, β)-plane for $d \in [0, 1, 2, 4]$ and $\delta \in [0, 0.25, 0.5, 0.75, 1]$. The dashed lines stand for the path of maximum virtual stiffness (see section VII).

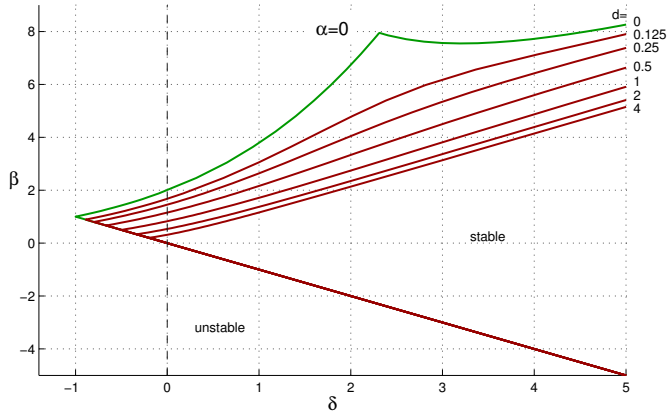

Fig. 6. The stability boundaries in the (δ, β)-plane for $\alpha = 0$ and $d \in [0, 0.25, 0.5, 1, 2, 4]$.

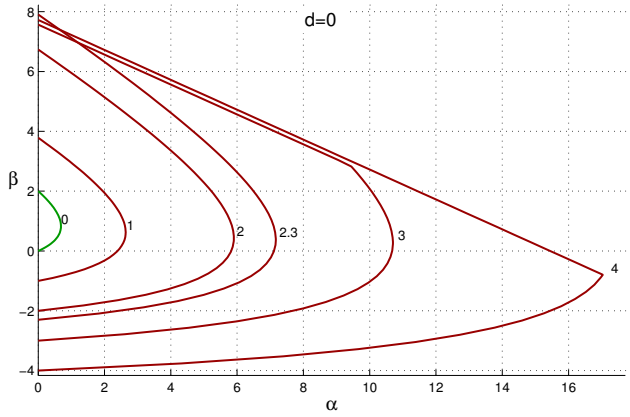

Fig. 7. The stability boundaries in the (α, β)-plane for the case $d = 0$ and large δ. A line with slope -0.5 is limiting the stable region from above for $\delta > 2.3$.

The normalized characteristic polynomial (17) depends just on four parameters, namely the normalized stiffness α, the normalized damping β, the physical damping δ and the time-delay factor d. So all physical parameters of the haptic device and variables of the virtual wall are expressed by normalized values. The following statements and conclusions are independent of the mass and the sampling time.

V. Stability Boundaries

The previous section derived a normalized characteristic polynomial of the control loop in Fig. 4 under utilization of the normalized parameters (14) and (16). This result together with the stability condition that all poles must lie inside the unit circle in the z-plane, allow determination of the stability boundaries. For practical purposes, the boundaries should be plotted in the (α, β)-plane, because these are the two parameters that are modified in the haptic simulation.

For fixed values of the delay factor $d \in [0, 1, 2, 4]$ and the physical damping $\delta \in [0, 0.25, 0.5, 0.75, 1]$ the stability boundaries are plotted in Fig. 5. On these boundaries at least one pole is lying on the unit circle, all others are inside. The poles and thus the stability boundaries are independent of the haptic device's mass and the time delay. The stable region is increasing for a higher physical damping δ. For negative $\alpha < 0$ the system becomes unstable. As the stability boundaries are computed iteratively, no analytic formula can be given here.

The lower starting point of each boundary lies at $(\alpha, \beta) = (0, -\delta)$, independent of the delay factor d. This dependency becomes obvious when looking at the stability boundaries for $\alpha = 0$ in the (δ, β)-plane in Fig. 6: the stable region is bounded by the line $\beta = -\delta$. Formulating this line as necessary stability condition with the non-normalized parameters yields

$$B \geq -b. \tag{19}$$

For zero stiffness $K = 0$, the virtual damping must be greater than the negative physical damping.

Remark 3: A special case occurs for $d = 0$ and $\delta > 2.3$. In the (α, β)-plane a line appears which is limiting the stable region besides the parabola-like stability boundary (see Fig. 7). This line appears only for $d = 0$.

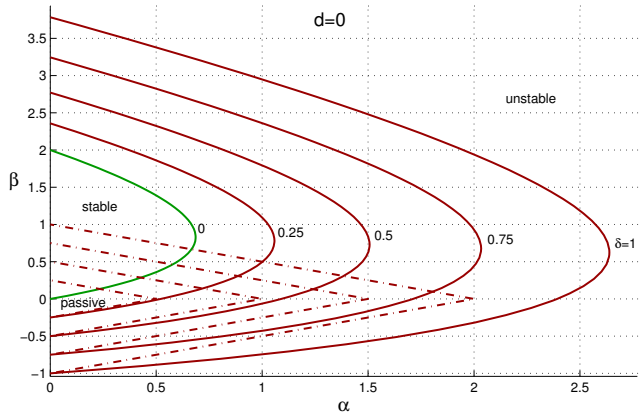

Fig. 8. The stability boundaries in the (α, β)-plane for the case $d = 0$ and $\delta \in [0, 0.25, 0.5, 0.75, 1]$. The dash–dotted lines represent Colgate's passivity condition.

VI. Comparison to the Passivity Condition

The passivity condition for $d = 0$ derived in [1]

$$b > \frac{KT}{2} + |B| \tag{20}$$

can be rewritten with the normalized parameters

$$\delta > \frac{\alpha}{2} + |\beta| \tag{21}$$

for $T > 0$ and $m > 0$. This condition is visualized as dash–dotted lines in the (α, β)-plane in Fig. 8 and in the (δ, β)-plane in Fig. 9. As was expected, the passive region is a subset of the stable region for $d = 0$. This corresponds to the fact that the passivity condition is conservative, [2].

If the passivity condition (21) is compared to the stability boundaries for $d > 0$, e.g. in Fig. 5, it becomes clear that this condition would specify a region which is crossing the stability boundary and is lying partly outside the stable region. Thus, the passivity condition holds only for $d = 0$. As in most haptic

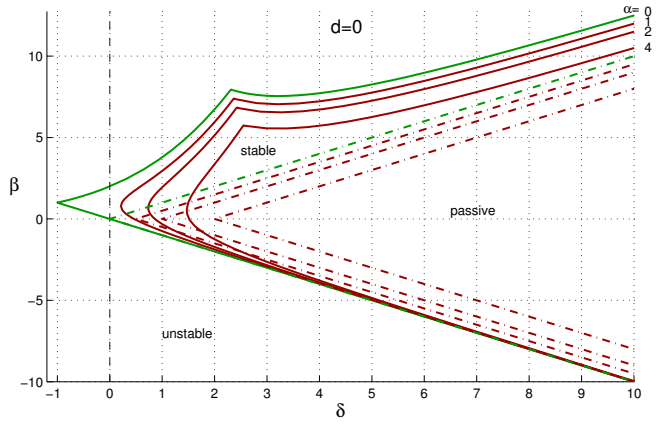

Fig. 9. The stability boundaries in the (δ, β)-plane for the case $d = 0$ and $\alpha \in [0, 1, 2, 4]$. The dash–dotted lines represent Colgate's passivity condition.

simulations some time delay occurs due to various reasons, the passivity condition (20) represents only a theoretical boundary. For real simulations where $d > 0$ it can not be applied.

VII. Maximum Virtual Stiffness

Rendering stiff walls is a core challenge in haptic simulations. This section discusses the influence of the physical damping on the maximum stable stiffness.

The stability boundaries in Fig. 5 are generated for fixed values of the delay factor d and the normalized physical damping δ. For each of these curves an (α, β)-value pair exists such that the normalized stiffness α is maximum, i.e. the rightmost point on each stability boundary. The virtual stiffness in that point will be denoted as α_{max}. A stiffness greater than α_{max} can not be stabilized by adopting the virtual damping β.

If these value pairs are connected for different values of the physical damping δ and fixed delays $d = const.$, a curve inside the (α, β)-plane can be drawn: the path for maximum virtual stiffness. This curve is plotted as dashed lines in Fig. 5.

Transforming this path into the (α_{max}, δ)-plane illustrates the influence of the physical damping δ on the maximum stable virtual stiffness α_{max}. Fig. 10 shows the resulting stability boundaries in two different scalings. Above these boundaries the system is unstable. Note that these curves are independent of the virtual damping β. It can been seen that the maximum stable stiffness α_{max} is increasing for a greater physical damping δ. Furthermore, the slope of the curve is increasing for smaller delays d.

For $\delta > 6$ it seems as if the dependency of the maximum stable virtual stiffness α_{max} on the physical damping δ becomes linear (Fig. 10 (b)). Assuming a linear dependency with slope g, the following equation can be stated,

$$\alpha_{max} = g \cdot \delta. \tag{22}$$

The slope g depends solely on the delay factor d. In non-normalized parameters this equation reads

$$K_{max} = g \cdot \frac{b}{T}. \tag{23}$$

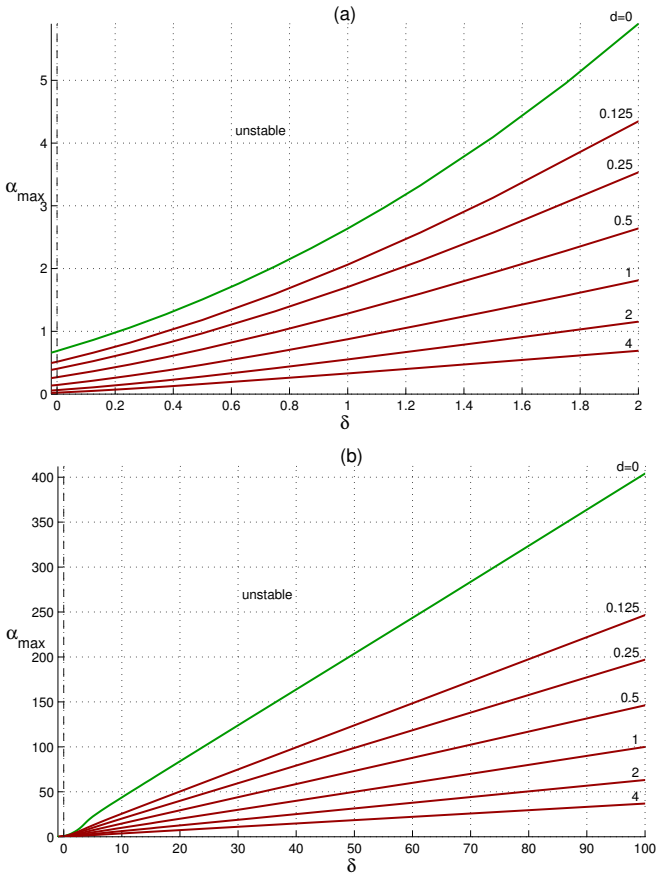

Fig. 10. The maximum stable virtual stiffness α_{max} for $d \in [0, 0.125, 0.25, 0.5, 1, 2, 4]$.

Thus, for (very) large values of the physical damping it seems as if the maximum stable stiffness depends linearly on the sampling rate $1/T$ and the physical damping b. It is independent of the haptic device's mass m.

Note that the system time delay $d \cdot T$ is proportional to the sampling period T. The linear dependency on the sampling rate $1/T$ in equation (23) implies a constant delay factor d.

Remark 4: For physically undamped systems $b = 0$ the dependency of the maximum stable stiffness was already derived in [9]. It depends quadratically on the sampling rate $1/T$ and linear on the mass m:

$$K_{max}(b = 0, d = 0) \approx 0.6863 \cdot \frac{m}{T^2}. \tag{24}$$

$$K_{max}(b = 0, d = 1) \approx 0.1445 \cdot \frac{m}{T^2}. \tag{25}$$

VIII. Example

In the previous section the dependency of the maximum stable stiffness on the physical damping was discussed. This section demonstrates the effects of an increasing physical damping using step responses. Consider therefore a haptic interface with the following properties similar to a PHANToM device [11]:

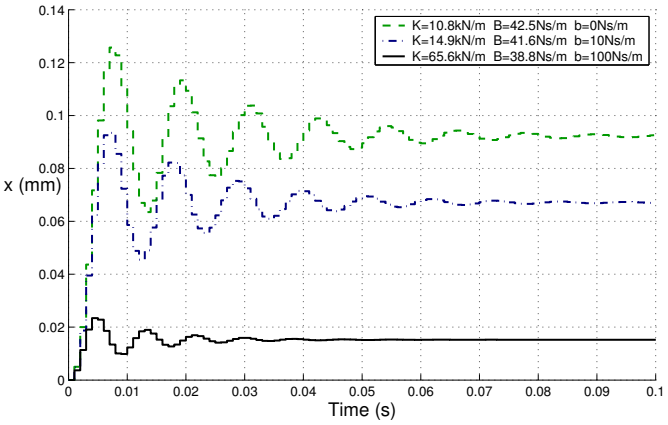

Fig. 11. Three step responses for $d = 1$, $m = 0.1kg$ and $T = 0.001s$.

Mass:	$m = 0.1kg$
Sampling Time:	$T = 0.001s$
Delay factor:	$d = 1$

The physical damping is assumed to be adjustable using three values $b = [0, 10, 100]\, Ns/m$, respective $\delta = [0, 0.1, 1]$. A stiff wall should be implemented with some stability margin. Thus, the virtual stiffness is set to 75% of its maximum stable value, i.e. $\alpha = [0.108, 0.149, 0.656]$. The virtual damping is left unchanged compared to the values needed to stabilize the system with the stiffness α_{max}, i.e. $\beta = [0.425, 0.416, 0.388]$ (compare with Fig. 5). For these parameters the step responses from force to position are shown in Fig. 11.

Although the stiffness for the system with the high physical damping $b = 100Ns/m$ is by factor 6 larger than for the undamped system, the highly damped system is settling faster.

The stiffness set for physically undamped systems is by factor 3 larger than those achieved by Massie and Salisbury ($K_{max} \approx 3.5kN/m$) for the PHANToM device in [11]. The main reason therefore is constituted in [12] as the velocity filter which results in an approximate lag of $50ms$. Therefore, it was not possible to set high values for the virtual damping.

IX. Conclusions

In this publication a discrete-time equivalent of the transfer function of a physically damped virtual mass is derived. It is used to determine the normalized stability boundaries for haptic rendering, whereby the virtual environment is represented by a time-discrete spring-damper system (discrete PD-controller). Thereafter, the path for maximum virtual stiffness was determined under utilization of the stability boundaries.

The following conclusions for the examined system can be summarized from above results:

- In the normalized parameter plane the stability boundary is independent of the haptic device's mass and the sampling period.
- As was expected, the Colgate's passivity condition derived in [1] defines a region inside the stability boundary for undelayed systems ($d = 0$). Yet, it cannot be applied for real haptic simulations for that time delay is present.
- Higher physical damping allows for larger stable virtual stiffness (monotonic behavior).
- For large values of the physical damping the maximum stable stiffness depends linearly on the sampling rate $1/T$ and the physical damping b.
- The minimum stable negative value for discrete damping corresponds to the physical damping, $B = -b$, independently of the sampling time and the time delay.

This paper focuses on the influence of the physical damping on the stability boundary. For future investigations, the approach presented in this publication could be extended to examine effects, like sensor and actuator quantization, signal noise or compliance of the haptic device. Furthermore, an analytical representation of the stability boundaries is missing. The passivity condition which is applicable for undelayed haptic interfaces should be generalized to systems with time delay.

X. Acknowledgment

The authors would like to thank Dr. Naim Bajcinca for the fruitful discussions. This paper would not be as it is without the suggestions he had.

References

[1] J. E. Colgate and G. Schenkel, "Passivity of a class of sampled-data systems: Application to haptic interfaces," in *1994 American Control Conference*. AIAA, 1994.

[2] J. Colgate and J. Brown, "Factors affecting the z-width of a haptic display," in *Proc. of the IEEE Int. Conf. on Robotics and Automation*, May 1994, pp. 3205–3210.

[3] B. Hannaford and J. Ryu, "Time-domain passivity control of haptic interfaces," in *Proc. of the IEEE Int. Conf. on Robotics and Automation (ICRA)*, 2001, pp. 1863–1869.

[4] J. Ryu, Y. Kim, and B. Hannaford, "Sampled and continuous time passivity and stability of virtual environments," in *Proc. of the IEEE Int. Conf. on Robotics and Automation (ICRA)*, 2003, pp. 822–827.

[5] J.-H. Ryu, C. Preusche, B. Hannaford, and G. Hirzinger, "Time domain passivity control with reference energy behavior," *IEEE Transactions on Control Systems Technology*, 2005.

[6] S. Salcudean and T. Vlaar, "On the emulation of stiff walls and static friction with a magnetically levitated input/output device," *ASME Journal of Dynamic Systems, Measurement and Control*, March 1997.

[7] R. J. Adams and B. Hannaford, "Stable haptic interaction with virtual environments," *IEEE Trans. on Robotics and Automation*, vol. 15, no. 3, pp. 465–474, June 1999.

[8] J. Gil, A. Avello, A. Rubio, and J. Flórez, "Stability analysis of a 1 dof haptic interface using the routh-hurwitz criterion," *IEEE Transactions on Control Systems Technology*, pp. 583–588, 2004.

[9] T. Hulin, C. Preusche, and G. Hirzinger, "Stability boundary and design criteria for haptic rendering of virtual walls," in *Proc. of the 8th International IFAC Symposium on Robot Control*, Bologna, Italy, September 2006.

[10] J. Mehling, J. Colgate, and M. Peshkin, "Increasing the impedance range of a haptic display by adding electrical damping," in *Proc. of the IEEE WorldHaptics Conference (WHC)*, Pisa, Italy, March 2005, pp. 257–262.

[11] T. Massie and J. Salisbury, "The phantom haptic interface: A device for probing virtual objects," in *Proc. of the ASME Winter Annual Meeting, Symposium on Haptic Interfaces for Virtual Environment and Teleoperator Systems*, Chicago, 1994, pp. 295–302.

[12] M. C. Cavusoglu, D. Feygin, and F. Tendick, "A critical study of the mechanical and electrical properties of the phantom haptic interface and improvements for high performance control," *Presence*, vol. 11, no. 6, pp. 555–568, 2002.